An echo top estimation using vertical interval interpolation

Maryna Lukach[1, 3], Maarten Reyniers[1], Oliver Salazar Celis[2, 3], Annie Cuyt[3]

[1]*Royal Meteorological Institute of Belgium, Ringlaan 3, B-1180 Ukkel, Belgium*
[2]*Avantage Reply, Belgium*
[3]*University of Antwerp, Middelheimlaan 1, B-2020 Antwerp, Belgium*

(Dated: 18 July 2014)

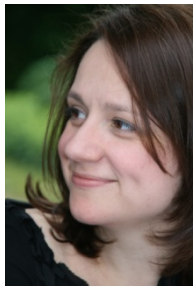

Maryna Lukach

1 Introduction

Radar echo tops were analyzed in meteorology from the moment the first weather radars were put into service, and even before the precise definition of an echo top was formulated. The first notation of the echo top definition belongs to Donaldson and can be found in a private conversation with Dr. David Atlas according to Lakshmanan et al., (2013). Donaldson suggested that a storm echo top is defined by the maximum height of some standard value of reflectivity. In the course of this particular study we define the echo top as the maximum height $H_{i,h}$ (in km AMSL) related to the measured echo $Z_{i,h} = \tau$ (in dBZ) at the i-th point of the measurements domain:

$$EchoTop_i = \max\left(\left\{H_{i,h} : Z_{i,h} = \tau\right\}\right), \qquad (1.1)$$

where h runs from some minimal height above the sea level $H_{\min}$ (1 km AMSL) up to the maximum height $H_{\max}$ that most often is taken as the tropopause top (20 km AMSL).

The echo top concept is widely used with different threshold values τ (18 dBZ, 38 dBZ or 45 dBZ) to detect strong updrafts of the storm that may point to potential severe weather such as hail (Waldvogel et al., 1979) and wind gusts. Unfortunately, the limitations of existing echo top calculation methods were recognized in different studies (e.g., Atlas et al., 1963; Delobbe and Holleman, 2006; and Lakshmanan et al., 2013).

The assignment of the height at which echo top appears is one of the sources of the possible errors. The error can occur due to inaccurate antenna pointing or to variations of the atmospheric propagation conditions. Another possible source of error is related to the measurement of the reflectivity itself. The latter is most often caused by attenuation and/or overshooting. Both types of errors tend to increase with the distance from the radar because of the increased size of the sampled volume. Except for the above-mentioned uncertainties, the probability that radar during the scanning cycle will detect reflectivity exactly equal to the given threshold is rather small. All the possible error sources were tackled in different articles (e.g., Delobbe and Holleman, 2006; and Lakshmanan et al., 2013; Atlas et al., 1963).

The height assignment problem was addressed in the study published by Delobbe and Holleman, (2006). The uncertainty in the height assignments was evaluated by comparison between the Belgian and Dutch radars in Wideumont and de Bilt, respectively. They conclude that: “The impact of the height assignment errors is very limited (around 0.5 km for all ranges). In contrast, small errors in the reflectivity measurements may strongly affect the echo top heights especially if the measured maximum reflectivity is close to the echo top threshold”.

In addition, the reflectivity Z reported at a certain location can be affected by the side-lobes artifacts and can be valid approximately a half-power beam width away, according to Atlas et al., (1963). A review of the existing solution of this problem can be found in Lakshmanan et al., (2013). In the same study an estimation of the echo top height, assuming a locally linear variation in the vertical reflectivity profile near the cloud top, was suggested. The assumption of local linearity also allows assessing the echo top in the domain points where reflectivity values in the h volumes are close but not exactly equal to the threshold τ.

The idea of this study is to test a technique that estimates the echo top exploiting not only the vertical but also the horizontal variation of reflectivity measurements. In this study, the assumption of local linearity is relaxed by allowing also non-linear variation of reflectivity vertically and horizontally.

A vertical segment interpolation technique, described in Section 3, is a suitable solution for this problem because it deals with measurement uncertainties in a very natural way. The generalized rational interpolating models can represent the echo top of any threshold based on the measurements of one or several radars, independently of their location and scanning strategy. To test the idea, data of a single radar are used. Description of the scanning strategy and the resolution of the data can be found in Section 2. Results of the experiment are presented and discussed in Section 4 of the paper.

2 Radar Measurements

For this experiment data from the volume scan of the C-Band (5.62 GHz) weather radar in Wideumont (Belgium) are used. The radar performs three scans: 1) a 5 elevation scan every 5 minutes, 2) a 10 elevation scan and 3) a velocity dedicated scan, both performed every 15 minutes. Measurements from the second volume scan are used in this study. In the second scan the radar sweeps the atmosphere at 0.5°, 1.2°, 1.9°, 2.6°, 3.3°, 4.0°, 4.9°, 6.5°, 9.4° and 17.5° elevation angles with a 483 Hz pulse repetition frequency. The samples are collected every 500 m in range, corresponding to an average of 2 successive range bins, and 1° in azimuth, corresponding to an average of 20 pulses. The maximum range of the radar measurements is 240 km. The data are coded with a resolution of 0.5 dB. Note that the Doppler filtering is not used in the second scan. Post-processing corrections of the raw radar data include identification of non-meteorological echoes based on: 1) satellite observations of cloud-free areas (Goudenhoofdt, 2014), 2) a texture-based technique (Gabella and Notarpietro, 2002); and 3) a three-dimensional algorithm as proposed in Steiner and Smith, (2002) and Berenguer et al., (2006). The effect of the post-processing corrections for the first elevation at 0.5° can be observed in Figure 1. The removed non-meteorological echoes are colored in grey.

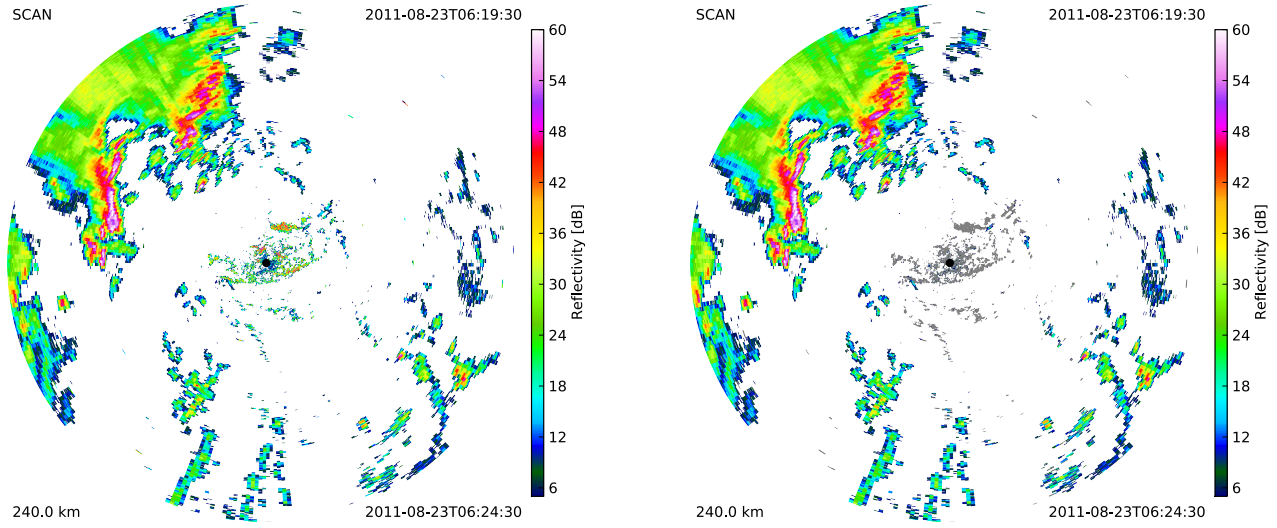

a) b)

Figure 1: The reflectivity data of the first elevation (0.5°), with the original uncorrected data panel a) and post-processed data panel b). Non-meteorological echoes eliminated from the scan are marked in grey.

After applying the post-processing corrections, the data of the volume scan are geo-localized. The latitude, longitude and height above the sea level, assuming 4/3 Earth's radius model (Doviak and Zrnic, 1993) are calculated for the center of each sample volume. Transformation of the position to the geographical coordinate system reduces errors in the composite grid of a large domain area.

3 Interpolation method

3.1 Theory and notation

The generalized rational multivariate interval interpolation technique (GRMIIT) used in the following is based on the idea described in Salazar Celis et al., (2007). The GRMIIT uses generalized rational functions of a finite dimensional real vector $\bar{x}$ of the form

$$r_{n,m}(\bar{x}) = \frac{p_{n,m}(\bar{x})}{q_{n,m}(\bar{x})} = \frac{\sum_{j=0}^{n} p_j b_j(\bar{x})}{\sum_{j=0}^{m} q_j b_j(\bar{x})} \qquad (3.1)$$

where the real numbers p_j and q_j represent the $n+1$ coefficients of the numerator and the $m+1$ coefficients of the denominator and where the $b_j(\bar{x})$ are multivariate basis functions. For the normalization, one of the coefficients p_j and q_j can be fixed and the rational function $r_{n,m}(\bar{x})$ will have n+m+1 degrees of freedom. In our meteorological application, $\bar{x} = (\phi,\lambda)$ where the real numbers ϕ and λ represent the latitude and the longitude of the radar measurement points. Furthermore, the Chebyshev polynomials of the first kind are used for $b_j(\bar{x})$ ordered in the following way: $b_0(\phi,\lambda) = 1$, $b_1(\phi,\lambda) = \phi$, $b_2(\phi,\lambda) = \lambda$, $b_3(\phi,\lambda) = 2\phi^2 - 1$, $b_4(\phi,\lambda) = 2\lambda^2 - 1$, $b_5(\phi,\lambda) = \phi\lambda$, $b_6(\phi,\lambda) = 4\phi^3 - 3\phi$, $b_7(\phi,\lambda) = 4\lambda^3 - 3\lambda$, $b_8(\phi,\lambda) = 2\phi^2\lambda - \lambda$, $b_9(\phi,\lambda) = 2\lambda^2\phi - \phi$, $b_{10}(\phi,\lambda) = 8\phi^4 - 8\phi^2 + 1$, ... How n and m are chosen is explained in the sequel.

Generalized rational functions of sufficiently low degree can already accurately approximate functions showing almost constant values in one region and a sharp increase/decrease in values in the other region. These exceptional approximation properties were demonstrated in different applications of the suggested method (e.g., Cuyt et al., to appear; Cuyt et al., 2014; Pacanowski et al., 2012; Deschrijver et al., 2010; Salazar Celis et al., 2013). In contrast to other nonlinear approximation techniques, the proposed vertical segment interpolation provides, by using uncertainty intervals F_i around each measurement at $\bar{x}_i$, full control of the residual error.

Consider a set of $s+1$ measured values $f_i, i = 0,...,s$ at positions $\bar{x}_i$, $i = 0,...,s$. Let the measurement uncertainty be represented by the real value intervals $F_i = \left[\underline{f_i}, \overline{f_i}\right]$ with $\underline{f_i} \le f_i \le \overline{f_i}$. We now search for a generalized rational function $r_{n,m}(\bar{x})$ of the form given in (3.1) that satisfies

$$r_{n,m}(\bar{x}_i) \in F_i, \quad i = 0,...,s$$

or (3.2)

$$\underline{f_i} \le r_{n,m}(\bar{x}_i) \le \overline{f_i}, \quad i = 0,...,s,$$

where $n + m \le s$.

Assuming $q_{n,m}(\bar{x}_i) > 0$, $i = 0,...,s$ and linearizing (3.2) we obtain the homogeneous system of linear inequalities

$$\begin{cases} p_{n,m}(\bar{x}_i) - \underline{f_i} q_{n,m}(\bar{x}_i) \ge 0 \\ -p_{n,m}(\bar{x}_i) + \overline{f_i} q_{n,m}(\bar{x}_i) \ge 0 \end{cases}, \quad i = 0,...,s. \qquad (3.3)$$

The assumption that $q_{n,m}(\bar{x}_i)$ is positive in the points $\bar{x}_i, i = 0,...,s$ causes no loss of generality.

Let us denote by $A_{n,m}$ the $(2s+2)\times(n+m+2)$ matrix corresponding to the inequalities in (3.3),

$$A_{n,m}=\begin{pmatrix} b_0(\bar{x}_0) & \cdots & b_n(\bar{x}_0) & -\underline{f_0}b_0(\bar{x}_0) & \cdots & -\underline{f_0}b_m(\bar{x}_0) \\ \vdots & & \vdots & \vdots & & \vdots \\ b_0(\bar{x}_s) & \cdots & b_n(\bar{x}_s) & -\underline{f_s}b_0(\bar{x}_s) & \cdots & -\underline{f_s}b_m(\bar{x}_s) \\ -b_0(\bar{x}_0) & \cdots & -b_n(\bar{x}_0) & \overline{f_0}b_0(\bar{x}_0) & \cdots & \overline{f_0}b_m(\bar{x}_0) \\ \vdots & & \vdots & \vdots & & \vdots \\ -b_0(\bar{x}_s) & \cdots & -b_n(\bar{x}_s) & \overline{f_s}b_0(\bar{x}_s) & \cdots & \overline{f_s}b_m(\bar{x}_s) \end{pmatrix} \qquad (3.4)$$

and by $A^{(j)}_{n,m}$ the j-th row of the matrix in (3.4). It was shown in Salazar Celis et al., (2007) that a robust solution $r_{n,m}(\bar{x})$ of (3.3) can be computed from the following quadratic programming problem:

$$\arg\min_{\bar{c}\in R^{n+m+2}} \|\bar{c}\|_2^2$$

$$\text{subject to} \qquad (3.5)$$

$$A^j_{n,m}\bar{c}-\delta\left\|A^j_{n,m}\right\|_2\geq 0,\quad j=1,...,2s+2$$

with $\bar{c}=\left(p_0,...,p_n,1,q_1,...,q_m\right)^T$ and $\|\ \|_2$ denoting the Euclidean norm. The real value $\delta>0$ is set to the inverse of the condition number of the matrix $A_{n,m}$ (Cuyt et al., 2014). If the quadratic programming problem (3.5) has a solution, it is unique and the function $r_{n,m}$ is pole-free at each measured point, meaning

$$\forall i=0,...,s,\ q_{n,m}(\bar{x}_i)>0. \qquad (3.6)$$

Existence of the solution for specific n and m depends on the width of the intervals F_i and on s. For $n+m=s$, a solution is guaranteed to exist (Cuyt and Wuytack, 1987). At the same time, several choices for n and m may deliver a generalized rational interpolant. So, while we may obtain a unique $r_{n,m}(\bar{x})$ for given n and m, we may find various interpolants when varying n and m. It is most natural to proceed with the search for a suitable n and m by increasing $n+m$, for instance by letting (n,m) run through the sequence (0,0), (1,0), (1,0), (2,0), (1,1), (0,2), (3,0), (2,1), (1,2), (0,3), (4,0), … In this way the first choice for n and m that leads to a solution of (3.5) delivers the least complex generalized rational function. For a more complete discussion of this aspect we refer to (Cuyt et al., 2014). Let us now discuss how to treat the data. The selection procedure for the radar measurements starts with the interpolation of the smallest vertical segments, being the most trusted measurements, and adaptively adds segments depending on the found solution. Details on how this is done, can be found in (Cuyt et al., to appear)

3.2 2D vertical segment interpolation of echo top

The volumetric measurements of Wideumont's weather radar are transformed into a set of uncertainty intervals for the height of a given echo top threshold of 45 dBZ. The width of each interval in a particular geographical point $\bar{x}_i=(\phi_i,\lambda_i)$ is assumed to be equal to the difference between two heights containing the threshold reflectivity.

As explained in Section 2, the volumetric radar measurements are post-processed and the available heights $H_{i,(h-1)}$ and $H_{i,h}$ corresponding to the closest reflectivities $Z_{i,(h-1)}$ and $Z_{i,h}$ enclosing the threshold value τ, $Z_{i,(h-1)}\geq\tau\geq Z_{i,h}$, are extracted. Here the index h runs through a number of discrete values corresponding to scanning elevations. For each of these points the geolocation $\bar{x}_i=(\phi_i,\lambda_i)$ is

calculated. The heights $H_{i,(h-1)}, i = 0,...,s$ and $H_{i,h}, i = 0,...,s$ are used to form vertical segments F_i. The lower bound $\underline{f}_i$ of vertical segment F_i takes the value of $H_{i(h-1)}$ and the upper bound $\overline{f}_i$ takes the value of H_{ih} for each of the $s+1$ points in the orthogonal projection on the 0° elevation scan plane having exceeded the threshold τ.

With this $\bar{x}_i$ and F_i we now apply the GRMIIT and compute $\bar{c}$ from (3.5) which are the coefficients in $r_{n,m}(\phi,\lambda)$ of (3.1).

The values $r_{n,m}(\phi_i,\lambda_i)$ represent the $EchoTop_i$ values of (1.1) in each of $s+1$ measurement points. This interpolation $r_{n,m}(\phi_i,\lambda_i)$ provides a rough resemblance of the $EchoTop_i$ values. For a more accurate solution a 3D problem with vertical segments representing the reflectivity measurement uncertainties could be considered.

4 Results and discussion

The results of the interpolating height of the reflectivity measurements of the Wideumont's radar for 23 August 2011 (at 0634 UTC) are presented in Figure 2. A set of 1506 vertical segments was selected by the procedure described in Section 3. The GRMIIT returns a $r_{n,n}(\phi,\lambda)$ function with $n+1=5$ numerator coefficients and $m+1=15$ denominator coefficients. The points $\bar{x}_i = (\phi_i,\lambda_i),\ i = 0,...,1505$ belong to the Wideumont's radar domain in the 240 km range from the (49.9136, 5.5044) location. The interval lower bounds $\underline{f}_i, i = 0,...,1505$ on the radar measurements domain vary between 0.6 km and 12.8 km AMSL. The interval upper bounds $\overline{f}_i, i = 0,...,1505$ vary from 0.7 km to 15.3 km AMSL. The coefficient vector $\bar{c}$, leading to the function $r_{4,14}(\phi,\lambda)$, is given in Table 1 (for the numerator coefficients p_j of $p_{4,14}(\varphi,\lambda)$) and in Table 2 (for the denominator coefficients q_j of $q_{4,14}(\phi,\lambda)$).

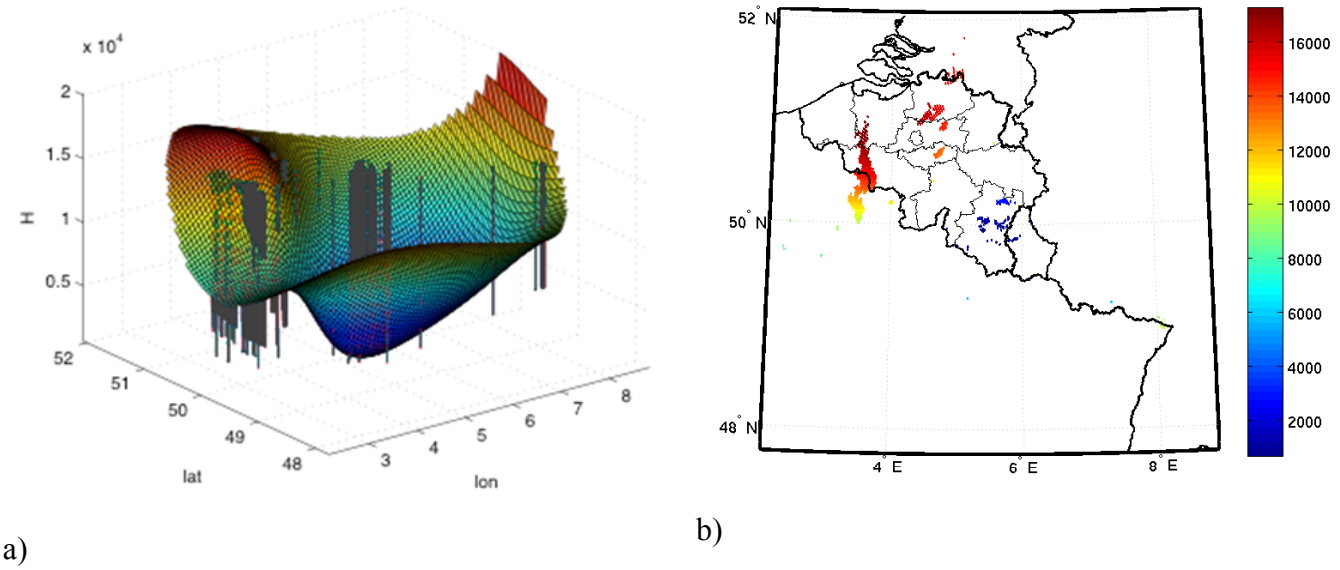

a) b)

Figure 2:The interpolating function $r_{4,14}$ with 1506 vertical intervals panel a) with the corresponding EchoTop (in m AMSL) panel b) ($\tau = 45$ dBZ).

Table 1: Coefficients of the numerator of the $r_{4,14}$ interpolation function.

p_j	Value
p_0	9.409398042650650
p_1	0.257886996070062
p_2	0.447830743881366
p_3	1.859853164522489
p_4	7.447515170159329

Table 2: Coefficients of the denominator of $r_{4,14}$ interpolation function.

q_k	Value
q_0	0.000686897833439
q_1	-1.30407311420512e-20
q_2	-9.33367062381218e-21
q_3	0.000048374525072
q_4	0.000439435209733
q_5	-4.20270574696356e-20
q_6	-0.000114693620535
q_7	0.000031177771540
q_8	-1.25748025952830e-20
q_9	2.24536641100569e-21
q_{10}	-0.000024860291922
q_{11}	6.32190581637592e-20
q_{12}	-0.000024860291922
q_{13}	-0.000024860291922
q_{14}	-0.000024860291923

To conclude, in this work we have presented a generalized rational multivariate interval interpolation technique and showed the results of its application to the echo top estimation. As can be observed in Figure 2, some residual artifacts of the ground clutter close to the radar location influence the echo top interpolation function. This emphasizes the importance of the assessment of the radar measurements. As mentioned in Section 3, the *EchoTop* achieved by this method is only a rough estimate of the true echo top values.

The application of GRMIIT may be extended to interpolation of the 3D radar reflectivity field. In such an application the vertical segments represent the uncertainty in the reflectivity measurement at each point (ϕ_i,λ_i,h_i) of the radar volumetric data. From the interpolation function $r_{n,m}(\phi,\lambda,h)$ the discrete level surface $r_{n,m}(\phi_i,\lambda_i,h_i) = 45$ provides a more precise echo top estimation. It will also allow

us to better assess the effects of both types of uncertainties (in height and in reflectivity) in the radar measurements.

Acknowledgement

The authors would like to acknowledge Edouard Goudenhoofd for his work on the quality of the radar data as well as Dieter Poelman and Loris Foresti for reviewing the manuscript.

References

Waldvogel A. and Federer, B. and Grimm, P. Criteria for the detection of hail cells // J. Appl. Meteor. - 1979. - 18. - pp. 1521 - 1525.

Delobbe L. and Holleman, I. Uncertainties in radar echo top heights used for hail detection // Met. Apps - 2006. - 13. - pp. 361 - 374.

Lakshmanan V. and Hondl, K. and Potvin, C. K. and Preignitz, D. An Improved Method for Estimating Radar Echo-Top Height // Wea. Forecasting - 2013 - 28. - pp. 481 - 488. : doi: http://dx.doi.org/10.1175/WAF-D-12-00084.1

Goudenhoofdt, E. Areal rainfall statistics based on a 10-year reanalysis of volumic radar observations // To be submitted - 2014

Gabella, M. and Notarpietro, R. Ground clutter characterization and elimination in mountainous terrain // Proceedings of ERAD - 2002 -Vol. 305.

Steiner, M. and Smith, J.A. Use of three-dimensional reflectivity structure for automated detection and removal of nonprecipitating echoes in radar data // J. Atm. and Ocean. Techn. - 2002 - 19 : Vol. 5. - pp. 673 - 686.

Berenguer, M. and Sempere-Tores, D. and Corral, C. and Sanchez-Diezma, R. A fuzzy logic technique for identifying nonprecipitating echoes in radar scans. // J. Atm. and Ocean. Techn. - 2006. - 23 (9). - pp. 1157 - 1180.

Doviak, R.J. and Zrnic, D.S. Doppler radar and weather observations. - Academic Press - 1993.

Salazar Celis, O. and Cuyt, A. and Verdonk, B. Rational approximation of vertical segments // Numer. Algorithms. - 2007. - 45. - pp. 375-88.

Salazar Celis, O. and Cuyt, A. and Deschrijver, D. and Vande Ginste, D. and Dhaene, T. Macromodeling of high-speed interconnects by positive interpolation of vertical segments // Applied Mathematical Modelling. - 2013. - 37. - pp. 4874-4882.

Deschrijver, D. and Dhaene, T. and Salazar Celis, O. and Cuyt, A. Rational modeling algorithm for passive microwave structures and systems. - Progress in industrial mathematics at {ECMI} 2010 Springer, Berlin - 2012. . - pp. 37-43.

Cuyt, A. and Salazar Celis, O. and Lukach, M. Multidimensional IIR filters and robust rational interpolation // Multidimensional Systems and Signal Processing - 2014. - 25. - pp. 447-471.

Cuyt, A. and Salazar Celis, O. and Lukach, M. and In't Hout, K. Analytic models for Parameter dependency in Option price modelling - to appear. - pp. 1-16.

Cuyt, A. and Wuytack, L. Nonlinear methods in numerical analysis // Mathematics studies 136, North-Holland, Amsterdam - 1987. - pp. 129-132.

Pacanowski, R. and Salazar Celis, O. and Schlick, C. and Granier, X. and Poulin, P. and Cuyt, A. Rational BRDF // IEEE Transactions on Visualization and Computer Graphics - 2012. - 18. - pp. 1824-1835.